


Leonard Hansen¹
Annett Wollmann^{1,*}
Martin Weers¹
Bernd Benker²
Alfred P. Weber¹

Triboelectric Charging and Separation of Fine Powder Mixtures

For increasingly finer powders, the material-specific separation at high loadings is a challenging task, for instance in recycling processes. Here, a combination of triboelectric charging and electrostatic separation was investigated for powder mixtures of talcum and calcite. The dependencies of the triboelectric charge on the mass loading, the gas velocity, and the mixture ratio were investigated. While higher charge levels were achieved with increasing gas velocity, the mass loading had an opposite effect on the net charge. Although bipolar charge distributions were observed within pure materials and mixtures, electrical neutralization did not occur in the mixtures. Therefore, already in a non-optimized setup, a decent degree of material enrichment (of up to 53 %) was found on the separating electrodes.

 This is an open access article under the terms of the Creative Commons Attribution License, which permits use, distribution and reproduction in any medium, provided the original work is properly cited.

Keywords: Fine powder, Mixtures, Separation, Triboelectric charging

Received: October 09, 2019; *revised:* February 12, 2020; *accepted:* February 13, 2020

DOI: 10.1002/ceat.201900558

1 Introduction

In pneumatic dry dispersion of powders, the numerous collisions of the particles with each other, and also with the walls, contribute to the desired dispersing effect but also induce triboelectric charging. Particle charging is used for electrostatic separation in the secondary raw materials sector, for material-specific sorting of metal/plastic or plastic/plastic quantities, and in the mineral raw materials sector [1], for processing potash crude salts [2–4]. In the ultra-fine range ($<20\ \mu\text{m}$), it is used for pharmaceuticals and in food technology [5–9]. In future recycling processes, e.g., the recovery of lithium from pyrometallurgical recycling of lithium-ion batteries, sorting techniques for such ultra-fine particles will also become necessary within the mineral materials sector [10–13].

While the charging mechanisms are complex and, to a large extent, still poorly understood, it is generally accepted that the difference in the work function of the contacting partners is the driving process for charge transfer [14]. In the field of plastic separation, so-called triboelectric series (TES) have been established, which may vary according to the contacting details, the surface properties, and the environmental conditions [15–17]. In elaborated experiments, it was observed that, in particle-particle collisions [18] and in particle-wall collisions [19], different polarities may occur even within the same material. By using the work function of small glass particles (typically $>20\ \mu\text{m}$) as fit parameter, Wang et al. [19] could nicely explain the observed dependence of the net charge on the composition of the binary glass powder mixtures.

In the range of fine non-conducting particles (diameter $<10\ \mu\text{m}$), which is in the focus here, only a few studies are available, with partly contradictory results. Based on Faraday cup electrometer (FCE) measurements, Mehrani et al. [20] have shown that the particle-wall collisions can lead to charge transfer and/or charge separation. However, as pointed out by Peart [21], such FCE measurements only deliver net charges. In contrast, Matsusaka et al. [22] performed charge measurements on single fine particles and corroborated a bipolar charge distribution even for pure materials [23]. Even more interesting from the material sorting point of view was their observation that no neutralization occurred in a mixture of oppositely charged powders (negative Al_2O_3 ($x_{50,0} = 3.9\ \mu\text{m}$) and positively charged fly ash ($x_{50,0} = 4.2\ \mu\text{m}$)).¹⁾

So far, only very dilute flow systems of fine powders (typically $<0.1\ \text{wt}\%$) have been investigated, identifying particle-wall collisions as the dominant charging process. Therefore, one objective of the present work is to study the triboelectric charging at higher mass loadings. The second goal is to investigate the possibility of sorting particles from an ultra-fine powder mixture according to the material.

¹⁾Leonard Hansen, Dr.-Ing. Annett Wollmann, Martin Weers, Prof. Dr. Alfred P. Weber
annett.wollmann@tu-clausthal.de
TU Clausthal, Institute of Particle Technology, Leibnizstrasse 19,
38678 Clausthal-Zellerfeld, Germany.

²⁾Dr.-Ing. Bernd Benker
Clausthal Research Centre for Environmental Technology (CUTEC),
Leibnizstrasse 23, 38678 Clausthal-Zellerfeld, Germany.

1) List of symbols at the end of the paper.

2 Materials and Methods

2.1 Materials

Two different powders were used for the experiments: calcite (CaCO_3) with a density of 2700 kg m^{-3} and a median particle size of $x_{50.3 \text{ calcite}} = 1.9 \mu\text{m}$ and talcum ($\text{Mg}_3\text{Si}_4\text{O}_{10}(\text{OH})_2$) with a density of 2800 kg m^{-3} and a median particle size of $x_{50.3 \text{ talcum}} = 5.1 \mu\text{m}$. The materials were used as pure substances and as mixtures. The corresponding particle size distributions were determined with a laser diffraction spectrometer (HELOS[®] KR, Sympatec) (see Fig. 4 below). Calcite showed a higher fine fraction with a maximum particle size of $10 \mu\text{m}$, whereas talcum contained particles up to $25 \mu\text{m}$. The size distributions of the mixtures ranged between those of the pure substances (see Fig. 4).

2.2 Methods

Fig. 1 presents an overview of the applied methods. These can be subdivided into two parts: triboelectric charging and electrostatic separation.

In order to analyze the triboelectric charging of the used particle system, various measurement methods were employed: total net charge (electrometer, Keithley 6514), net charge per size class (electrical low pressure impactor (ELPI) (ELPI+, Dekati)), and particle size distribution (HELOS[®] and ELPI+).

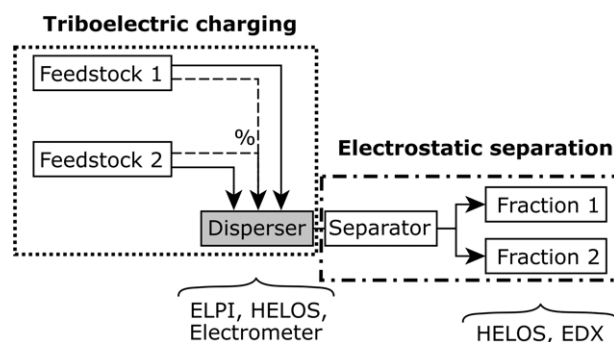


Figure 1. Overview of the experimental setup (frames detailed in Figs. 2 and 3).

Subsequent to the charging, the particles were separated in an electrostatic precipitator. The detailed experimental setups of both components will be described in the following sections.

2.2.1 Dispersing and Charging System

The particles were charged in a dry disperser (RODOS[®], Sympatec), which is based on the injector principle (Fig. 2a). It is a common dispersion unit used in combination with laser diffraction measurement systems.

The powder, either pure materials or mixtures, was fed to the dispersion and charging system using a rotary disk feeder,

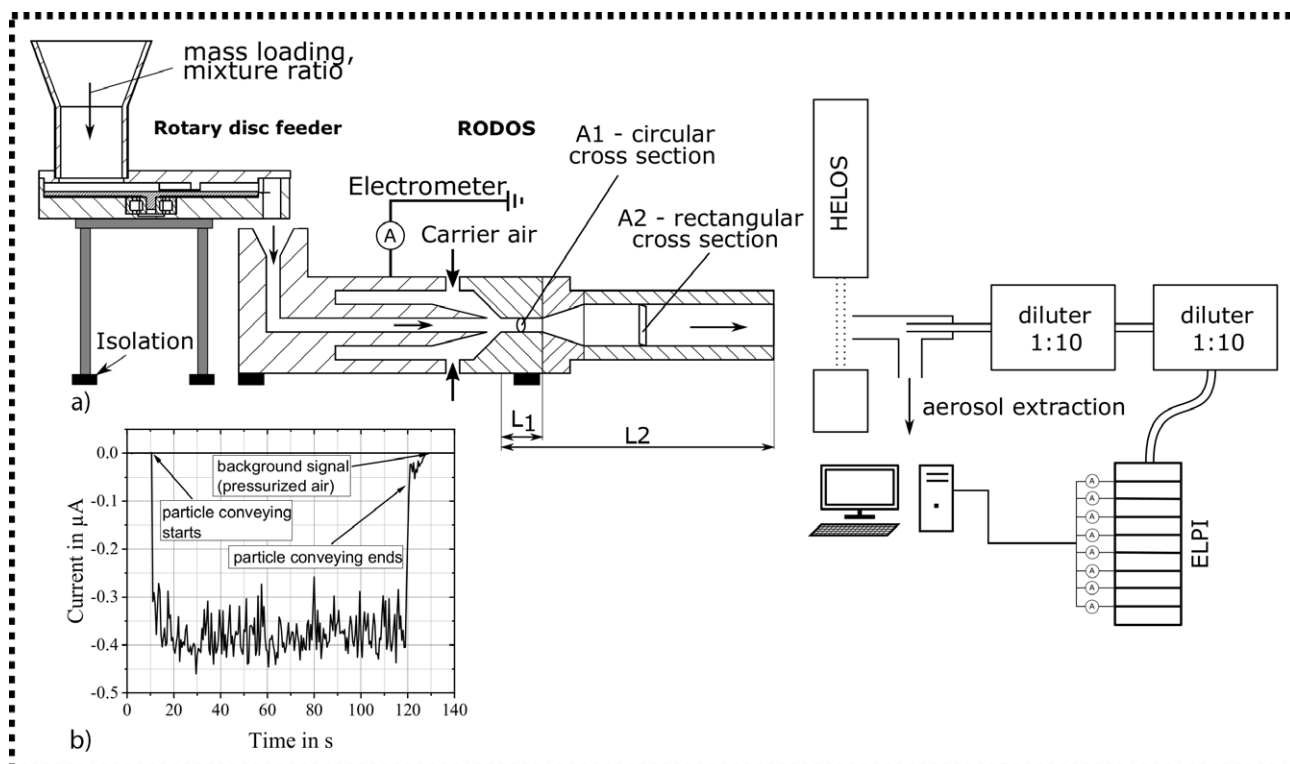


Figure 2. (a) Experimental setup for particle dispersion, particle charging, and characterization of the triboelectric charge of the powder (the dotted frame refers to Fig. 1). (b) Raw current signal of the electrometer, attached to the RODOS[®] (constant mass flow: 0.11635 g s^{-1} ; material: calcite; pressure: 2.5 bar).

whereby the mass flow was varied in the range from 0.01 to 0.15 g s^{-1} , corresponding to a mass loading of about 0.3–5 wt %.

The particle flow within the RODOS[®] is mixed with dried compressed air (8 % relative humidity). The mixing ratio of the compressed dispersion air to the aspired powder-loaded ambient air was at least 20:1. Thus, the triboelectric charging process is not affected by the relative humidity of the ambient air.

To analyze the total net charge of the particles, the RODOS[®] setup was isolated and grounded via an electrometer, which recorded the current, induced by particle-wall collisions. The gas flow rate entering the system was varied by adjusting the carrier air inlet pressure. For the experiments described here, an inlet pressure of 2.5 bar was mostly used, corresponding to a gas flow rate of 190 L min^{-1} . Only for the experiments with different gas velocities, the carrier air pressure was varied (see Fig. 5b below). Within the RODOS[®] system, agglomerates are destroyed by a combination of acceleration, shear forces, and particle-wall collisions, which together with the high volumetric gas flow prevents any particle deposits inside the disperser [24]. Moreover, the RODOS[®] was cleaned by pressurized air before every measurement.

A raw current signal can be seen in Fig. 2b. The nearly constant current signal indicates a virtually constant powder conveyance within the measurement time.

At the outlet of the RODOS[®], the particle size distribution was measured with a laser diffraction spectrometer to check the correct dispersion of the particles. The ELPI+, described in Sect. 2.2.2, was used to measure the particle net charge in the individual size classes. The side stream to the ELPI+ is sampled non-isokinetically from the main particle stream at a flow rate ratio of 1:100, realized with two serial dilution stages (each with a dilution ratio of 1:10).

2.2.2 Electrical Low-Pressure Impactor

The size-resolved charge measurements were performed with an ELPI. The impactor consists of 15 stages, which allow an in situ evaluation of the particle size distribution, covering a diameter range from 6 nm to $10 \mu\text{m}$.

To minimize bouncing effects [25], greased aluminum foils were used as collecting substrate. The aerosol volume flow rate through the impactor was kept constant with a critical nozzle (10 L min^{-1}). The size classification of the ELPI is based on inertial impaction and is therefore completely independent of the particle charge. The particle charge, which was given to the particles before entering the cascade impactor using a unipolar corona charger, was used to quantify the number of particles deposited on each stage. By switching off the charger, the ELPI was used to measure the native particle charge in each size class. This native charge, however, was the result of the triboelectric charging of the particles.

2.2.3 Electrostatic Separator

To separate the particles in the electric field, a separating apparatus with a quadratic cross-section

($s = H = 5 \text{ cm}$) and a length of 1.0 m was used, where the electrodes were 0.75 m long and started after an inlet zone of 0.25 m (Fig. 3). The aerosol inlet was located in the middle of the channel, and slot inlets for the sheath flow were integrated at both outer edges. The suction blower installed behind the cyclone ensured a constant total volume flow rate of $30 \text{ m}^3 \text{ h}^{-1}$, resulting in a dilution ratio of sheath air to aerosol flow of approximately 25:1. For these conditions, the flow inside the separator was assumed to be turbulent ($Re = 11\,734$). The particles leaving the separator were collected in a cyclone and analyzed offline. The particles adhering to the electrodes were sucked off by a lance attached to a vacuum cleaner and collected on a paper filter (50 mm in diameter). In addition to the pure powders, mixtures of calcite and talcum (70:30 wt %, 50:50 wt %) were used as feed materials for the separation.

The fraction in the cyclone and the deposited particles on the electrodes were evaluated regarding their size distribution by laser diffraction and regarding their elemental composition by energy dispersive X-ray (EDX) spectroscopy. For the laser diffraction measurements, the particles were conveyed in a wet suspension, dispersed and stabilized.

3 Experiments and Results

The results of the experimental investigations are divided into two main sections: (i) powder dispersion and triboelectric charging and (ii) electrostatic separation of pure powders and of mixtures. While the observations for the particle net charge will be presented and discussed first (Sect. 3.1), some important aspects of the particle charging become only accessible in the separation process (Sect. 3.2).

3.1 Dispersing and Triboelectric Charging

The setup shown in Fig. 2a was used to disperse and to charge powders of different compositions and different mass loadings. The measured particle size distributions for the used mixtures, as measured by laser diffraction at the RODOS[®] outlet, are shown in Fig. 4. It becomes obvious that the size distributions of the powder mixtures are mere superpositions of the constituent powders, indicating that processes such as hetero-agglomeration of calcite and talcum particles do not arise in the feed to a notable degree.

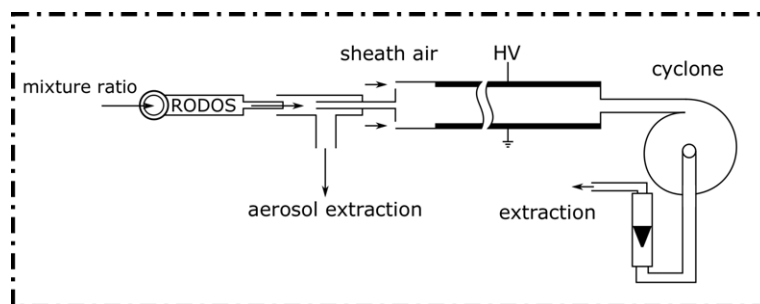


Figure 3. Experimental setup: electrostatic separator (the dashed-dotted frame refers to Fig. 1).

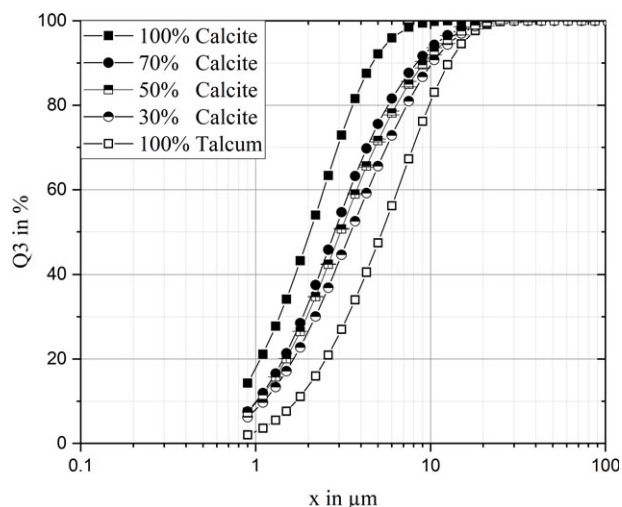


Figure 4. Particle size distributions of the used powders measured with laser diffraction (dry); arithmetic standard deviation of five measurements: $SD = 0.9\%$.

3.1.1 Influence of the Particle Mass Flow and the Material Mixture on Triboelectric Charging

In order to investigate the influence of the powder mass loading, different mass flow rates were realized. In addition, mixtures of different calcite/talcum ratios were used, as indicated by the weight fraction ranging from 0:100 wt % (pure talcum) to 100:0 wt % (pure calcite). The corresponding mass flow rates of the rotary disc feeder were determined gravimetrically. The experimental setup is identical to the RODOS[®] from Fig. 2a where the net powder charge was deduced from the measured current produced in the disperser due to particle-wall collisions.

Fig. 5a shows the mass-specific net charge ($\mu\text{C g}^{-1}$) as a function of the mass loading ($\text{mass}_{\text{particle}}$ per mass_{air}) for both the pure materials and the mixtures.

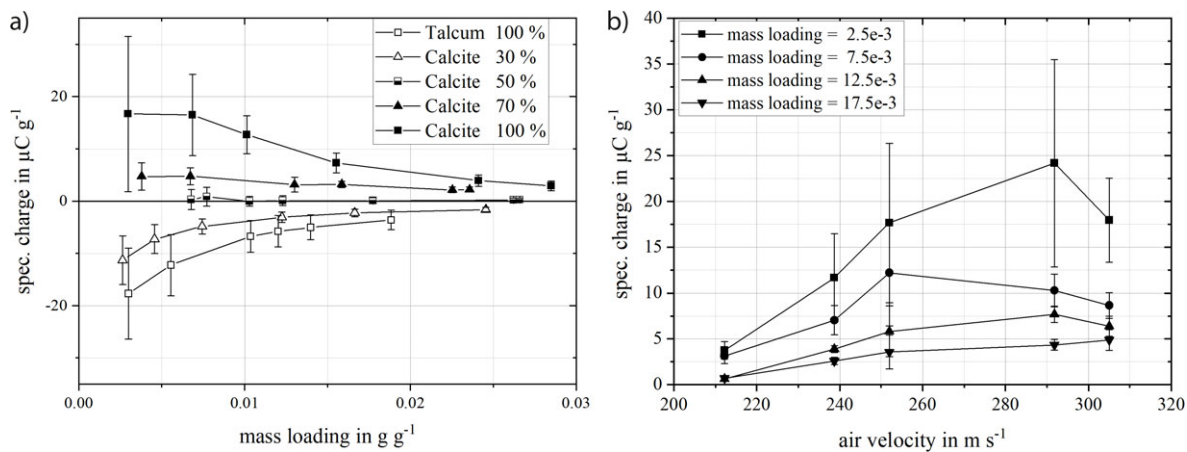


Figure 5. (a) Mass-specific charge of talcum and calcite particles as a function of the mass loading at different mixture ratios (mass flow air = 4.085 g s^{-1} , corresponding to an applied air pressure p of 2.5 bar). (b) Absolute value of the specific charge of the talcum particles as a function of the air flow velocity in the RODOS[®] disperser and the mass loading.

Calcite particles charge themselves triboelectrically with a different sign than talcum particles. At different mixing ratios, a decrease in the amount of specific charge up to a mixing ratio of 50 wt % calcite to 50 wt % talcum was observed, where this mixture appears to be neutral.

At the lowest investigated mass loading of 0.003 g g^{-1} , the specific charges of the two pure materials calcite and talcum have a similar level in the range of approximately $\pm 17.5 \mu\text{C g}^{-1}$ but different polarities. However, in both cases, the specific charge of the particles decreases with increasing mass loading. This behavior can be observed for the pure materials as well as for the mixtures. In powder pneumatic conveying experiments, Watano et al. [26] also found a decrease of the specific charge of poly(methyl methacrylate) (PMMA) particles with increasing particle mass flow. Based on a numerical simulation of the particle motion, they concluded that the number of collisions between particles increased with increasing loading, leading to a decrease in the possibility of particles colliding with the pipe wall [26]. From the comparison of experiments and simulations, which showed the same influence of the air velocity on the specific charge, they assumed that mainly the number of particle-wall collisions and the vertical component of the impact velocity determined the electrification of the particles [26]. To test this hypothesis in the present work, the air velocity was varied for different loadings of talcum powder. The results presented in Fig. 5b agree qualitatively with the findings of Watano et al. [26], although the absolute values are different, which may be due to the different material combination (talcum-stainless steel), the much higher air velocity ($> 200 \text{ m s}^{-1}$ vs $10\text{--}40 \text{ m s}^{-1}$), but mainly also due to the much smaller particles (5 vs $300 \mu\text{m}$). As shown in Fig. 5b, with higher velocity, the specific charge increases to a certain level and decreases again, similar to the behavior observed by Watano et al. [26]. This drop at high velocities is supposed to be due to a decrease of the number of particle-wall collisions as a consequence of the increasing particle motion parallel to the wall [26]. However, regarding the absolute particle charge, Watano et al. [26] found that the specific particle charge in the experiment was about one order of magnitude smaller than in the simulation. While

differences between experiment and model (e.g., only a two-dimensional discrete-element method (DEM) model, only one-way coupling [26]) may contribute to this discrepancy, another cause could be the way of particle charge measurement. In fact, when using an FCE, only the net charge of the powder is determined and possible bipolarities are therefore not taken into account, as will be shown in Sect. 3.2.

3.1.2 ELPI Measurements

The previous charge measurements were carried out for complete particle collectives using the electrometer attached to the RODOS[®]. In order to investigate how the particles were charged across the different size classes, measurements with the ELPI were performed with the charger switched off, obtaining the pure triboelectric particle charge. However, since the ELPI measurements were done after a 1:100 dilution (see Fig. 2a), a comparison of the total charge obtained with the RODOS[®] electrometer and the ELPI was done to check whether the diluter and tube system had affected the ELPI charge measurements. In Fig. 6a, the RODOS[®] electrometer results are compared with the ELPI measurements without charger (summed up over all stages) for calcite, talcum, and a 50-wt % mixture of both. Good agreement is found, with the exception of the talcum results which are placed above the ideal correlation (indicated by the dashed line). Since the ELPI has an upper cut-off of about 10 μm , approximately 20 wt % of the large talcum particles do not reach the device (see the talcum size distribution in Fig. 4). As indicated in Fig. 6b, these particles are likely to carry a negative charge, which explains the observed difference to the ideal correlation.

During the experiments, the corona charger of the ELPI was clocked, i.e. switched on and off. Fig. 6b shows the charge measurements over the different impactor stages for calcite, talcum, and a 50-wt % mixture of both. It is observed that the polarity of the net charges is reversed above a certain particle size for both talcum and calcite. Large talcum particles carry a negative net charge and large calcite particles carry a positive net charge, whereas particles smaller than 600 and 300 nm, respectively,

carry charges with the opposite sign. Besides the material, the work function of the particles depends also on their size and, even for particles of the same material, it has been predicted that small particles tend to charge negatively, and larger particles positively [27]. However, for a given material, the change of the work function from a 100-nm particle to a 10- μm particle is in the order of a few 0.01 eV [28], which cannot explain the extent of the polarity differences observed here.

Investigations by Kwetkus and Sattler [28] lead the way to another explanation of the observed effects. By performing repeated contacts of a metallic stamp with a fixed particle layer, they have shown that the polarity of the particles changed with an increasing number of contacts, firstly going into the direction of equilibration of the work functions, but later going into the opposite direction [29]. Based on the visual change of the powder appearance, they concluded that the particle surface changes either by oxidation or by mass transfer between stamp and particles [29]. By combining the observations made here in Figs. 5 and 6, it is hypothesized that the reason for the size dependency of the net charge shown in Fig. 7 is that smaller particles undergo fewer and less energetic collisions with the stainless-steel tube of the disperser. Due to higher inertia, the larger particles have a higher probability to reach the wall in the turbulent air flow, with higher vertical impact velocity and/or with a higher number of collisions. These more intense collisions with the wall may also promote mass exchange and/or chemical reactions with the wall. In addition, frictional effects due to the tangential velocity component during contact may also contribute to the particles charging [30] but have not been taken into account in the simulation [26] and the perpendicular contact experiments [29].

3.2 Electrostatic Separation

The main objective of this work is to separate fine particles according to the material in an electric field after a controlled triboelectric charging. Thereby it is assumed that the particle charge is obtained in the disperser and only charge separation occurs in the plate capacitor apparatus (see Fig. 3). However, as

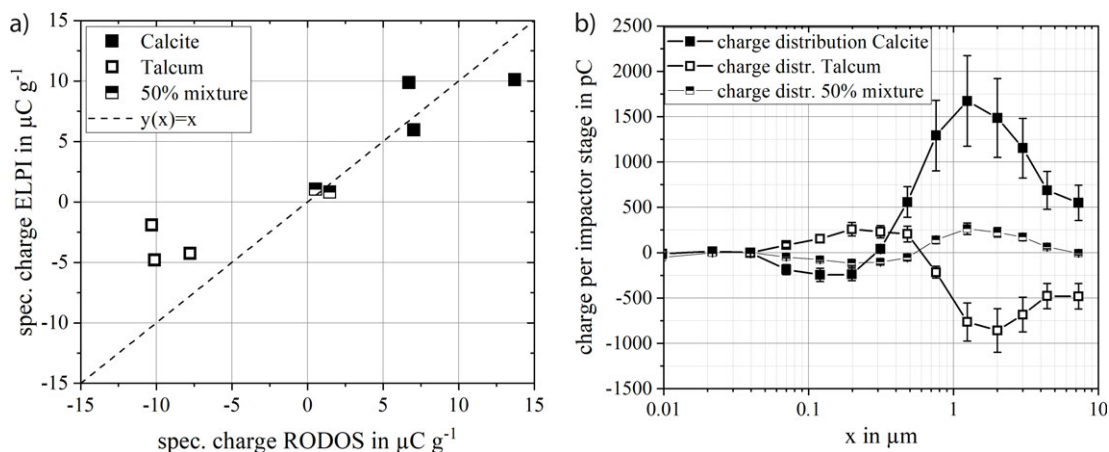


Figure 6. (a) Plausibility diagram between the collective and the ELPI measurements. (b) Charge distribution of talcum and calcite on the impactor stages.

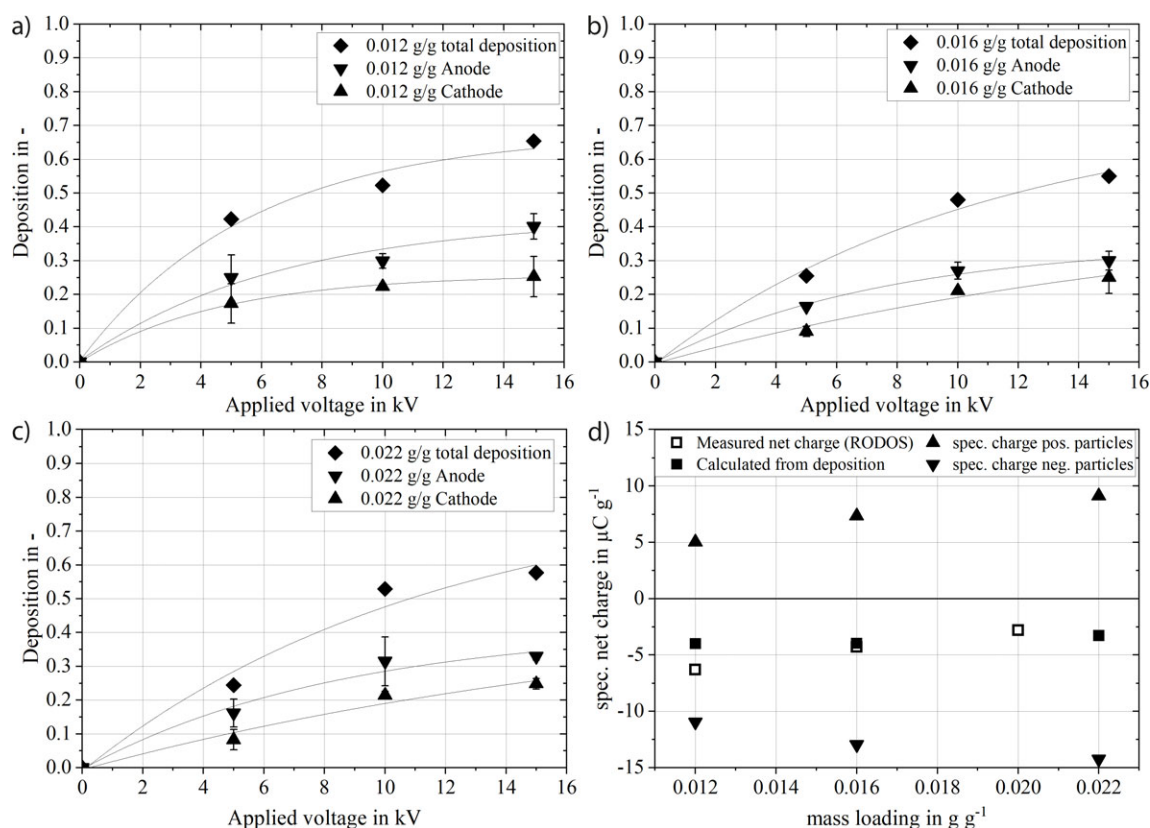


Figure 7. (a–c) Deposition efficiency as a function of the applied voltage for three different mass loadings (0.012, 0.016, and 0.022 g g⁻¹). (d) Calculated effective particle charge from the deposition of talcum (from the bipolar particle charge distribution, the net charge is calculated and compared to the measured RODOS[®] net charge).

will be shown below, the net charges determined with the electrometers of RODOS[®] and ELPI+ are not relevant for this separation, since even the pure materials exhibit a strong bipolar particle charging.

3.2.1 Mass Flow-Dependent Separation Efficiency

The deposition results in dependence on the applied voltage are shown in Fig. 7 for three mass loadings. While in all cases an increase of the deposition efficiency with the applied voltage is observed, the deposition efficiency tends to decrease with increasing mass loading. Since the gas flow in the separation apparatus is turbulent, the well-known Deutsch approach for electrostatic precipitators was applied to evaluate the data (adapted according to [30]).

$$E_{+/-}(x) = \alpha_{+/-}(1 - \exp(-D)) \quad (1)$$

where E is the degree of deposition and D is the Deutsch number, defined as [30]:

$$D = \frac{wL}{sv} = \frac{\Delta U \bar{q}_s^2 L}{s^2 3\pi \eta x V} \quad (2)$$

On the one hand, the values of D and $\alpha_{+/-}$ can be obtained by fitting Eq. (1) to the data in Fig. 7. On the other hand, from

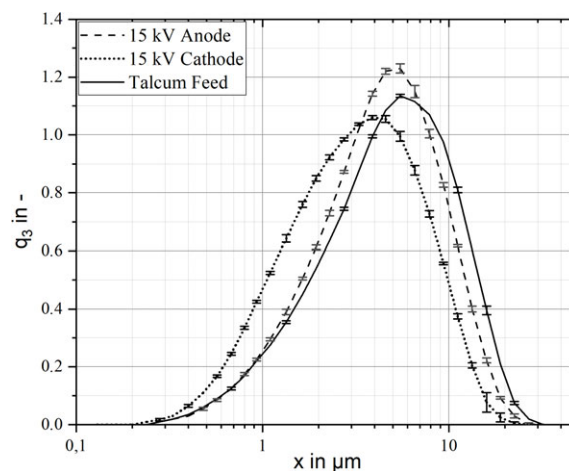


Figure 8. Density size distribution (q_3) of the deposited particles on both the anode (dashed line) and the cathode (dotted line) in the separator at an applied voltage of 15 kV and a mass flow of 0.012 g g⁻¹ of pure talcum (feed – solid line).

the measured size distribution $q_{3+/-}(x)$ of the powders deposited on the anode and the cathode (see Fig. 8) the separation curves can also be calculated by Eq. (3), using the feed density size distribution $q_{3, \text{feed}(x)}$:

$$E_{+/-}(x) = \frac{\alpha_{+/-} q_{3+/-}(x)}{q_{3,\text{feed}}(x)} \quad (3)$$

Hence, the charge per particle can be calculated from the deposited mass on the electrodes and the Deutsch number, due to the summation of the particle size classes. While the particle charges obtained from the deposition curves are much higher than the net charges measured with the RODOS[®] electrometer, the sum of the positive and negative charges and the numbers of neutral particles passing the precipitator agree well with the electrometer data. From the separation point of view, however, only the effective particle charges are important. The effective (bipolar) charges increase slightly with increasing powder mass loading, in contrast to the net charge.

The analyzed size distributions of the deposited pure talcum particles at both electrodes are compared with the feed size distribution in Fig. 8.

At both electrodes, small particles, as well as larger ones, were deposited. The mass concentration of smaller particles is clearly increased at the negative electrode, and the larger particles were preferentially deposited at the opposite electrode. This measurement underlines the bipolar charging behavior at different particle sizes of the pure materials. The fine talcum particles are rather positively charged, whereas the larger ones carry a negative net charge (see Fig. 6b), which implies a rather sharp separation. In contrast to this expectation, the size distributions on the electrodes are significantly overlapping (Fig. 8), which indicates that even within a given size class a bipolar charge distribution occurs. Therefore, the underlying charging mechanism not only depends on the particle size but may also be influenced by other factors, such as different particle surface properties and/or the type of particle-wall collision (e.g., the ratio of normal impact to sliding friction). Compared to the feed size distribution, a decent fraction of the largest particles ($x > 15 \mu\text{m}$) is lost due to settling within the separator.

3.2.2 Material-Dependent Powder Separation

Fig. 9 shows the particle size distributions of the particles deposited on the electrodes at an applied voltage of 5 kV. Also, the size distributions of the pure feed powders and of the mixture feeds are included. It is obvious that the size distributions of the deposited powders are shifted towards the pure materials. By calculating a separation curve for the pure substances, the purity of talcum on the anode is 83 % for the 50-wt % mixture feed and 77 % for the 70:30-wt % mixture feed, respectively.

However, since the powders exhibit bipolar charge distributions, the enrichment of the components was investigated with additional EDX characterization. In the EDX analysis, the ratios of the magnesium to the calcium content in the pure substances as well as in the mixtures and deposited particles at the electrodes, marked with E+ (anode) and E- (cathode), are shown in Fig. 10.

As expected, the content shifted towards talcum on the positive electrode and towards calcite on the negative electrode, at an applied voltage of 5 kV. The talcum content was increased by 53 % for the 50-wt % feed mixture and by 22 % for the 70:30-wt % feed mixture. Since pure talcum contained also 10 % calcium, it can be assumed that the talcum content was even higher. These results show that, during triboelectric charging of a 50 % mixture at high mass loadings, the particles are not neutralized by mutual particle-particle collisions. A sufficient charge remains to enrich the materials at the electrodes.

4 Conclusions

With the focus on the separation of mixtures, experiments on the triboelectric charging of aerosols were performed. The investigated materials are the insulators talcum and calcite in the size range of about 0.04 up to 20 μm . They can be efficiently triboelectrically charged by a disperser, with material-dependent polarity. Regarding the net charge, it was observed that small particles carried the opposite polarity compared to the large particles.

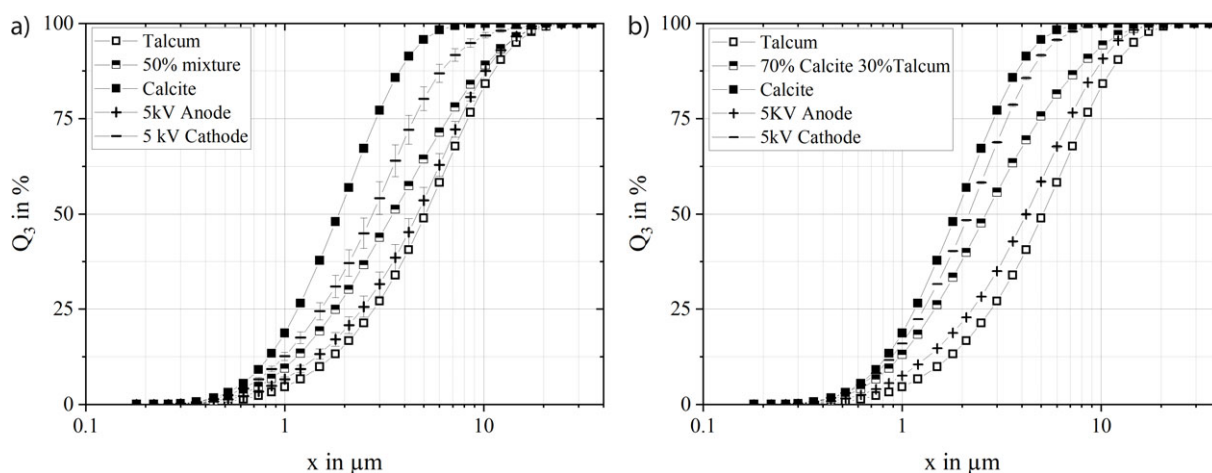


Figure 9. Particle size distribution of the deposited particles on the electrodes for feeding material mixtures of (a) 50 wt % calcite and (b) 70 wt % calcite; arithmetic standard deviation of two measurements: $SD = 0.3 \%$.

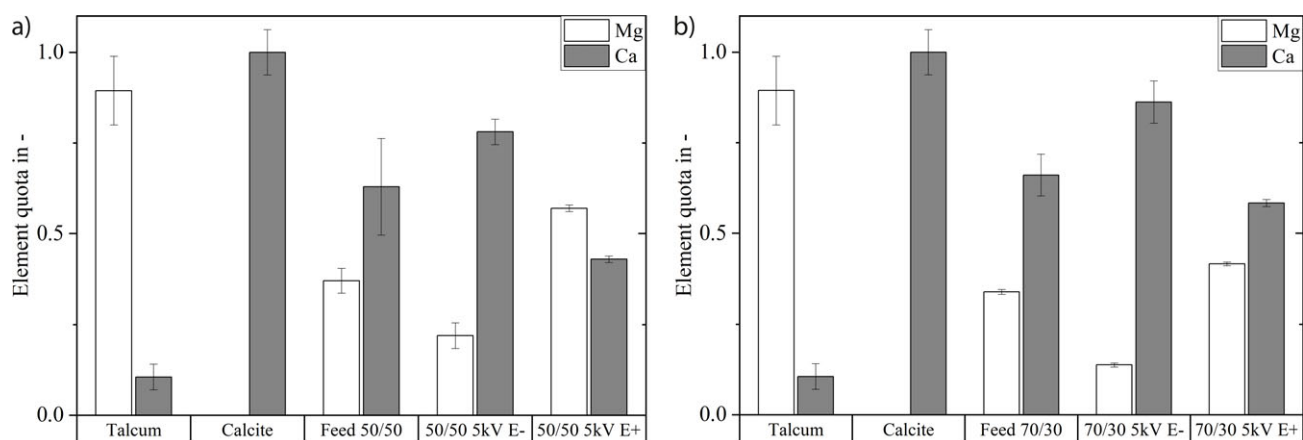


Figure 10. EDX analysis of the magnesium and calcium fractions in the deposited material on the electrodes for a feed mixture of (a) 50 wt % calcite and (b) 70 wt % calcite.

Neither for pure materials nor for mixtures neutralization effects did occur. Therefore, it is possible to separate a mixture of two triboelectrically charged insulator materials in an electric field at high mass loadings of approximately 1.3 wt %. A significant enrichment was achieved on the anode and the cathode, e.g., 53 wt % enrichment of talcum on the anode for a 50-wt % mixture of calcite and talcum.

In addition, the effective (bipolar) particle charge increases with the mass loading while the net charge was hardly influenced. For the separation process, only the effective particle charge is decisive, while the net charge may at best give a qualitative indication of the polarity changes for different materials.

Acknowledgment

The authors thank the German Research Foundation (DFG) for the financial support of this work within the SPP2045 priority program (WE 2331/22-1), and the group of Prof. Einar Kruijs (University of Duisburg-Essen), for providing the ELPI measurements.

The authors have declared no conflict of interest.

Symbols used

D	[-]	Deutsch number
$E_{+/-}$	[-]	grade of deposition on the positive and negative electrodes
H	[m]	height of the precipitator
L	[m]	length of the capacitor plates
\bar{q}	[C]	average charge of the particle
q_3	[-]	density size distribution
s	[m]	distance between the capacitor plates
SD	[%]	standard deviation
ΔU	[V]	applied voltage
\dot{V}	[m ³ s ⁻¹]	volumetric air flow rate
v	[m s ⁻¹]	mean gas velocity, $\dot{V} s^{-2}$

w	[m s ⁻¹]	particle migration velocity towards the electrodes
x	[m]	particle size

Greek letters

$\alpha_{+/-}$	[-]	deposited mass fraction on the positive and negative electrodes
η	[Pa s]	dynamic viscosity

Abbreviations

EDX	energy dispersive X-ray
ELPI	electrical low pressure impactor
FCE	Faraday cup electrometer

References

- [1] R. Köhnlechner, S. Sander, *BHM, Berg- Hüttenmänn. Monatsh.* **2009**, *154* (4), 136–139. DOI: <https://doi.org/10.1007/s00501-009-0453-2>
- [2] A. Singewald, G. Fricke, *Chem. Ing. Tech.* **1983**, *55* (1), 39–45. DOI: <https://doi.org/10.1002/cite.330550111>
- [3] J. Haeberle, A. Schella, M. Sperl, M. Schröter, P. Born, *Soft Matter* **2018**, *14*, 4987–4995. DOI: <https://doi.org/10.1039/c8sm00603b>
- [4] P. M. Ireland, *Powder Technol.* **2019**, *348*, 70–79. DOI: <https://doi.org/10.1016/j.powtec.2019.03.019>
- [5] H. Grosshans, M. V. Papalexandris, *J. Fluid Mech.* **2017**, *818*, 465–491. DOI: <https://doi.org/10.1017/jfm.2017.157>
- [6] H. Grosshans, M. V. Papalexandris, *Eur. Phys. J.: Appl. Phys.* **2018**, *82*, 11101. DOI: <https://doi.org/10.1051/epjap/2018170360>
- [7] N. Schwindt, U. von Pidoll, D. Markus, U. Klausmeyer, M. V. Papalexandris, H. Grosshans, *J. Loss Prev. Process Ind.* **2017**, *49*, 461–471. DOI: <https://doi.org/10.1016/j.jlp.2017.05.028>
- [8] H. Grosshans, M. V. Papalexandris, *Powder Technol.* **2017**, *315*, 227–235. DOI: <https://doi.org/10.1016/j.powtec.2017.04.012>

- [9] M. Rowland, A. Cavocchi, F. Thielmann, J. Kulon, J. Shur, R. Price, *Pharm. Res.* **2019**, *36*, 15. DOI: <https://doi.org/10.1007/s11095-018-2544-9>
- [10] T. Georgi-Maschler, B. Friedrich, R. Weyhe, H. Heegn, M. Rutz, *J. Power Sources* **2012**, *207*, 173–182. DOI: <https://doi.org/10.1016/j.jpowsour.2012.01.152>
- [11] G. Harper, R. Sommerville, E. Kendrick, L. Driscoll, P. Slater, R. Stolkin, A. Walton, P. Christensen, O. Heidrich, S. Lambert, A. Abbott, K. Ryder, L. Gaines, P. Anderson, *Nature* **2019**, *575*, 75–85. DOI: <https://doi.org/10.1038/s41586-019-1682-5>
- [12] C. Hanisch, T. Loellhoeffel, J. Diekmann, K. J. Markley, W. Haselrieder, A. Kwade, *J. Cleaner Prod.* **2015**, *108*, 301–311. DOI: <https://doi.org/10.1016/j.jclepro.2015.08.026>
- [13] O. Velázquez-Martínez, J. Valio, A. Santasalo-Aarnio, M. Reuter, R. Serna-Guerrero, *Batteries* **2019**, *5* (4), 68. DOI: <https://doi.org/10.3390/batteries5040068>
- [14] E. Németh, *Triboelektrische Aufladung von Kunststoffen*, Ph.D. Thesis, TU Bergakademie Freiberg, Freiberg **2003**.
- [15] D. K. Davis, *J. Phys. D: Appl. Phys.* **1969**, *2* (11), 1533–1537. DOI: <https://doi.org/10.1088/0022-3727/2/11/307>
- [16] M. W. Williams, *J. Macromol. Sci., Rev. Macromol. Chem.* **1976**, *14* (2), 251–265. DOI: <https://doi.org/10.1080/15321797608065771>
- [17] J. Henniker, *Nature* **1962**, *196*, 474. DOI: <https://doi.org/10.1038/196474a0>
- [18] K. M. Forward, D. J. Lacks, R. M. Sankaran, *Phys. Rev. Lett.* **2009**, *102*, 028001. DOI: <https://doi.org/10.1103/PhysRevLett.102.028001>
- [19] H. Wang, F. Fotovat, X. T. Bi, J. R. Grace, *Particuology* **2019**, *43*, 101–109. DOI: <https://doi.org/10.1016/j.partic.2018.07.001>
- [20] P. Mehrani, H. T. Bi, J. R. Grace, *Powder Technol.* **2007**, *173*, 73–81. DOI: <https://doi.org/10.1016/j.powtec.2006.11.021>
- [21] J. Peart, *KONA* **2001**, *19*, 34–45. DOI: <https://doi.org/10.14356/kona.2001009>
- [22] S. Matsusaka, M. Oki, H. Masuda, *Powder Technol.* **2003**, *135–136*, 150–155. DOI: [https://doi.org/10.1016/S0032-5910\(03\)00160-8](https://doi.org/10.1016/S0032-5910(03)00160-8)
- [23] S. Watano, S. Saito, T. Suzuki, *Powder Technol.* **2003**, *135–136*, 112–117. DOI: [https://doi.org/10.1016/S0032-5910\(03\)00159-1](https://doi.org/10.1016/S0032-5910(03)00159-1)
- [24] D. Langer, *Konstruktionsmethodische Entwicklung eines Trockendispersierers*, Ph.D. Thesis, TU Clausthal, Clausthal-Zellerfeld **2009**.
- [25] H. Kuuluvainen, A. Arffman, E. Saukko, A. Virtanen, J. Keskinen, *J. Aerosol Sci.* **2013**, *55*, 104–115. DOI: <https://doi.org/10.1016/j.jaerosci.2012.08.007>
- [26] C. F. Gallo, W. L. Lama, *J. Electrostat.* **1976**, *2* (2), 145–150. DOI: [https://doi.org/10.1016/0304-3886\(76\)90005-X](https://doi.org/10.1016/0304-3886(76)90005-X)
- [27] D. M. Wood, *Phys. Rev. Lett.* **1981**, *46*, 749. DOI: <https://doi.org/10.1103/PhysRevLett.46.749>
- [28] B. A. Kwetkus, K. Sattler, *J. Phys. D: Appl. Phys.* **1992**, *25* (10), 1400–1408. DOI: <https://doi.org/10.1088/0022-3727/25/10/004>
- [29] P. M. Ireland, *J. Electrostat.* **2012**, *70*, 524–531. DOI: <https://doi.org/10.1016/j.elstat.2012.08.004>
- [30] H. Schubert, *Handbuch der Mechanischen Verfahrenstechnik*, 1st ed., Wiley-VCH, Weinheim **2003**.